Dynamic behavior of boron carbide

T. J. Vogler, W. D. Reinhart, and L. C. Chhabildas

Citation: Journal of Applied Physics **95**, 4173 (2004); doi: 10.1063/1.1686902
View online: http://dx.doi.org/10.1063/1.1686902
View Table of Contents: http://scitation.aip.org/content/aip/journal/jap/95/8?ver=pdfcov
Published by the AIP Publishing

Dynamic behavior of boron carbide

T. J. Vogler,[a] W. D. Reinhart, and L. C. Chhabildas
Sandia National Laboratories, Solid Dynamics and Energetic Materials, P.O. Box 5800, MS 1181, Albuquerque, New Mexico 87185

(Received 12 September 2003; accepted 23 January 2004)

Boron carbide displays a rich response to dynamic compression that is not well understood. To address poorly understood aspects of behavior, including dynamic strength and the possibility of phase transformations, a series of plate impact experiments was performed that also included reshock and release configurations. Hugoniot data were obtained from the elastic limit (15–18 GPa) to 70 GPa and were found to agree reasonably well with the somewhat limited data in the literature. Using the Hugoniot data, as well as the reshock and release data, the possibility of the existence of one or more phase transitions was examined. There is tantalizing evidence, but at this time no phase transition can be conclusively demonstrated. However, the experimental data are consistent with a phase transition at a shock stress of about 40 GPa, though the volume change associated with it would have to be small. The reshock and release experiments also provide estimates of the shear stress and strength in the shocked state as well as a dynamic mean stress curve for the material. The material supports only a small shear stress in the shocked (Hugoniot) state, but it can support a much larger shear stress when loaded or unloaded from the shocked state. This strength in the shocked state is initially lower than the strength at the elastic limit but increases with pressure to about the same level. Also, the dynamic mean–stress curve estimated from reshock and release differs significantly from the hydrostate constructed from low-pressure data. Finally, a spatially resolved interferometer was used to directly measure spatial variations in particle velocity during the shock event. These spatially resolved measurements are consistent with previous work and suggest a nonuniform failure mode occurring in the material.
[DOI: 10.1063/1.1686902]

I. INTRODUCTION

Boron carbide (B_4C) is an intriguing material because of its low density and high strength. The boron carbide used is primarily in the chemical form B_4C; a good review of its physical properties can be found in Thévenot.[1] The shock behavior of B_4C has been studied by several researchers through the years as reviewed by Dandekar.[2] These studies showed that the Hugoniot elastic limit (HEL) of B_4C is 14–19 GPa, which is the highest reported for a ceramic.[3] Recent work on sleeved rods impacted with graded-density impactors[4] has revealed the elastic limit of B_4C at strain rates intermediate to planar impact and Hopkinson bar experiments. However, comparisons by Grady[5] with estimated hydrostatic compression curves for B_4C suggest that all or almost all of this strength is lost at stresses somewhat above the HEL, say 30–40 GPa. Similarly, work by Bourne[6] with lateral gauges suggested a significant loss of strength even below the HEL due to arrival of a ''failure wave.'' An alternate explanation for the apparent collapse of the Hugoniot to the hydrostat is the presence of a phase transition.[2,5] Further evidence of phase transformations has been found by an analysis of shock velocity data.[7] Finally, heterogeneous deformation mechanisms, such as cracks, cleavages, and melting zones, have been suggested by experiments with inclined mirrors[8] and by irregularities in interferometer readings.[5]

In the current work, time-resolved plate impact experiments were designed to measure the Hugoniot response of B_4C and the reshock and release paths followed. We use these experiments to assess the material for one or more phase transitions. Since the reshock and release experiments probe the material in states close to the Hugoniot state, they should be more suited to the detection of phase transitions with small volume changes. In addition, the reshock and release results are analyzed to directly determine the shear stress and strength retained in the shocked state. Finally, we report direct measurements of heterogeneous deformation obtained with the recently developed spatially resolved interferometry system.[9]

II. EXPERIMENTAL METHODS

The boron carbide used in the present investigation is the same as that studied by Dandekar.[2] It was produced using hot pressing techniques by Cercom, Inc., Vista, CA, and has a nominal grain size of 15 μm and an average density of 2.508 g/cm^3, implying either a porosity of about 0.5% or a slightly boron-rich composition (theoretical maximum density is 2.52 g/cm^3). Ultrasonic studies have determined the dependence of wave speeds on both porosity[10] and on the stoichiometry of boron carbide.[11] The longitudinal and shear wave speeds reported for this material were 13.49 and 8.65 km/s, respectively.[2] Based on these measurements, values of 432 GPa for Young's modulus and 0.15 for Poisson's ratio were calculated. Spall strength was found to depend upon the

[a]Electronic mail: tjvogle@sandia.gov

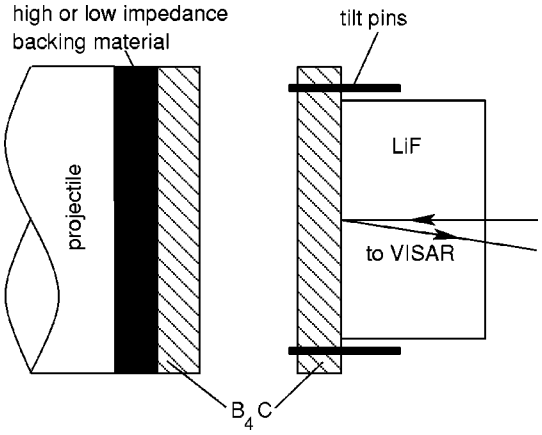

FIG. 1. Schematic of setup for reshock and release experiments.

stress level of initial loading with values from 0.24 to 0.46 GPa measured.[2] This is similar to the 0.4–0.5 GPa reported by Grady[3] but lower than the 0.59–0.77 GPa of Winkler and Stilp.[12] Additionally, a dependence of the spall strength on the pulse width was found.[2] Ultrasonic measurements performed at Sandia National Laboratory, Albuquerque, N. M., revealed spatial variations in the local sound speed and average values of about 13.7 km/s and 8.7 km/s for c_L and c_S, respectively. It is not clear whether the variations of sound speed are due to porosity or variations in chemical content.

Plate impact experiments were conducted using three different guns[13] for different velocities: a 50 or 63 mm bore gas gun for velocities to about 1 km/s, an 89 mm bore powder gun for velocities to about 2.3 km/s, and a 28 mm bore two-stage light gas gun for velocities from 1.8 to 7 km/s. The basic experimental configuration is shown in Fig. 1 with dimensions chosen to assure uniaxial strain conditions for the central region of the specimen for the duration of the experiment. The boron carbide target is backed by a lithium fluoride window,[14] which is of optical quality and is lapped and polished to be flat to within a few bands of sodium light. One surface of the window is diffused and approximately 100 nm of aluminum is vapor deposited before it is glued to the target. The impactor is a layer of boron carbide, copper, or tantalum. For many experiments, the B_4C impactor was backed with a high (copper or tantalum) or a low (TPX-polymethylpentene) impedance material to obtain the reshock or release behavior from the initial shocked state.

The projectile velocity on powder gun and air gun shots was measured with three electrical self-shorting pins to an accuracy better than 0.5%, while additional pins measure impact planarity. The two-stage gun incorporates an optical system to measure projectile velocity to an accuracy better than 0.2%. The particle velocity history at the target–window interface is measured using a velocity interferometer, velocity interferometer system for any reflector (VISAR).[15] The Doppler shift interference fringes measured with VISAR are converted to a velocity history. The velocity amplitude resolution is approximately 2% per interference fringe, and typically two to three fringes are achieved in the initial shock loading front. In most cases, two different fringe constants are used in the same experiment to yield unambiguous velocity histories.

III. HUGONIOT RESULTS

A total of seventeen plate impact experiments have been conducted to date as summarized in Table I. Of these, one was on the air gun, and four were on the powder gun. Of those from the two-stage gun, six were designed as reshock experiments and six for release. VISAR velocity histories for six release experiments on the two-stage gun are shown in Fig. 2, while those for four reshock experiments are shown

TABLE I. Summary of plate impact specimens.

Specimen	V (km/s)	Impactor material(s)	Impactor/target thickness (mm)	c_L (km/s)	HEL (GPa)	σ_h (GPa)	u_h (km/s)	ρ_h (g/cm^3)	U_s^p (GPa)
BC-I[a]	0.984	Ta	2.096/4.999	14.01	16.6	20.5	0.654	2.654	8.45
BC-II[b]	1.446	Cu	thick/8.024	14.02	18.0	24.9	0.866	2.725	8.87
BC-III[b]	1.706	Cu	thick/8.026	14.03	17.7	30.0	1.028	2.761	9.47
BC-IV[b]	1.960	Cu	thick/8.029	14.01	16.6	34.5	1.199	2.808	10.11
BC-V[b]	2.258	Ta	1.50/8.026	14.02	17.4	46.3	1.592	2.914	10.70
BC-VI[c]	1.851	B_4C/TPX	1.268/3.018	14.01	16.6	27.8	0.926	2.725	9.87
BC-VII[c]	2.652	B_4C/TPX	2.007/2.997	14.00	15.9	39.2	1.326	2.832	10.49
BC-VIII[c]	3.183	B_4C/TPX	2.032/3.023	13.99	15.8	47.3	1.592	2.903	10.90
BC-IX[c]	3.641	B_4C/TPX	2.022/3.020	13.98	15.2	54.3	1.821	2.966	11.17
BC-X[c]	4.175	B_4C/TPX	2.016/2.992	13.99	15.5	62.9	2.088	3.040	11.42
BC-XI[c]	4.789	B_4C/TPX	2.017/3.018	13.95	13.4	73.3	2.395	3.123	11.83
BC-XII[c]	1.803	B_4C/Ta	1.273/3.005	13.99	16.3	27.2	0.902	2.718	9.60
BC-XIII[c]	2.628	B_4C/Ta	1.963/3.015	13.89	15.7	39.2	1.314	2.823	10.93
BC-XIV[c]	3.228	B_4C/Cu	2.021/3.023	14.00	15.9	48.1	1.614	2.908	10.94
BC-XV[c]	3.647	B_4C/Cu	2.032/3.023	13.99	15.5	54.4	1.824	2.966	11.18
BC-XVI[c]	4.236	B_4C/Cu	2.042/3.018	?[d]	?[d]	62.9[d]	2.088[d]	3.040[d]	11.42[d]
BC-XVII[c]	4.885	B_4C/Cu	2.014/3.018	?[d]	?[d]	73.3[d]	2.395[d]	3.123[d]	11.83[d]

[a]Conducted on gas gun.
[b]Conducted on powder gun.
[c]Conducted on two-state gun.
[d]Elastic precursor not measured; Hugoniot state assumed from similar release experiment.

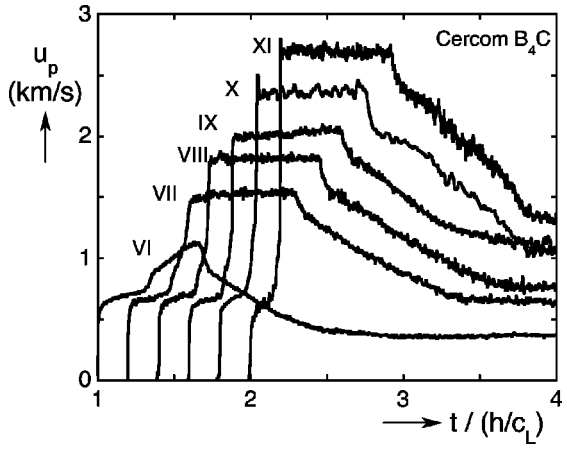

FIG. 2. Particle velocity history profiles from VISAR for B_4C release experiments (normalized time shifted in increments of 0.2 for clarity).

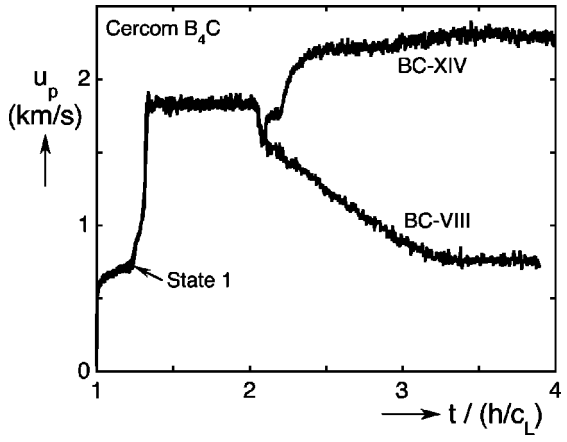

FIG. 4. Particle velocity history profiles for companion reshock and release experiments BC-VIII and BC-XIV.

in Fig. 3. All times plotted are normalized with respect to the elastic traversal time of that specimen to allow specimens of different dimensions to be more easily compared (values of c_L used in normalization can be found in Table I). Omitted from Fig. 3 are two experiments for which a Hugoniot state could not be calculated. For comparison, one reshock and one release experiment (BC-VIII and BC-XIV) conducted at the same impact velocity are shown in Fig. 4. The elastic wave, shock arrival time, and peak particle velocity are identical for the two experiments. The unloading and reloading histories differ, of course; these will be discussed later. Good agreement for initial loading is typical for the companion reshock and release experiments. Velocity histories for four shock loading experiments from the powder gun and one from the air gun are shown in Fig. 5. The experiments in Figs. 2 and 3 share three characteristics: an elastic wave with a window velocity of 0.6–0.7 km/s, a reverberation of the elastic wave with a velocity of about 1.0 km/s, and a plastic wave whose magnitude and velocity increases with increased shock stress. Similar features are seen for the experiments in Fig. 5.

The HEL was determined by impedance matching techniques between the sample and the LiF window based on the point in the VISAR history where the slope first begins to decrease immediately after the elastic shock. The measurements of HEL fell into two groups: the powder gun specimens at about 17.3 GPa, and the two-stage gun at about 15.4 GPa. Both are within the range of values reported previously,[3,10,12,16,17] but the difference is surprising. For the experiments shown in Fig. 5, a drop in measured velocity follows the initial elastic wave. This drop is, to our knowledge, unique amongs polycrystalline ceramics,[3] though similar behavior is observed in single crystal LiF (Ref. 18) and sapphire.[19,20] In contrast, a gradual rise in particle velocity is seen for the two-stage experiments such as those in Fig. 4, behavior similar to that of ceramics, such as SiC (Ref. 5) and Al_2O_3.[21] Note that the drop is observed in thicker specimens, while the gradual rise occurred for thinner specimens. Thus, the phenomenon is not due to precursor attenuation. Still, the two behaviors lead to very similar particle velocities just prior to arrival of the plastic wave and yield similar Hugoniot states (see Table I) for experiments that exhibited the two different behaviors at the HEL (e.g., samples BC-V and BC-VIII). Since the two groups of samples were produced by the same manufacturer, the reason for the differ-

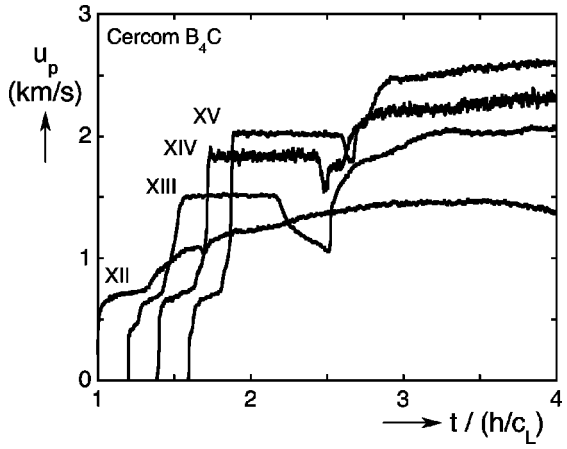

FIG. 3. Particle velocity history profiles from VISAR for B_4C reshock experiments (normalized time shifted in increments of 0.2 for clarity).

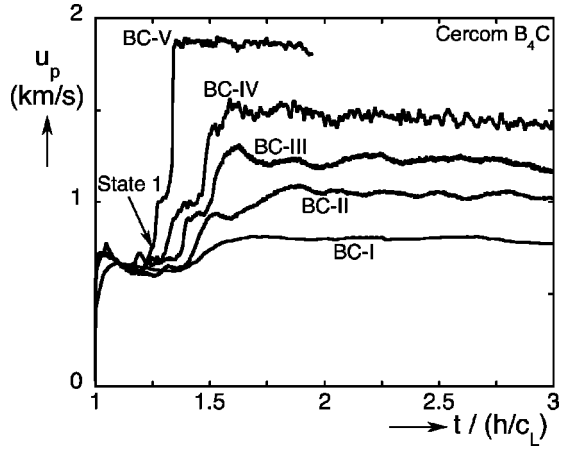

FIG. 5. Particle velocity history profiles from VISAR for experiments BC-I to BC-V conducted on the gas gun and powder gun.

ence at the HEL is unclear but is believed to be a consequence of batch-to-batch material variation or sample machining.

The Hugoniot state is calculated from the measured velocity history. The elastic wave is used as a fiducial by assuming the elastic wave speed follows a linear relationship with particle velocity as suggested by Grady[7] of:

$$c_L = c_L^o + 0.65u, \tag{1}$$

where c_L^o is the ambient sound speed of 13.7 km/s, u is the particle velocity associated with the elastic wave at the HEL, and the linear coefficient of 0.65 was obtained by Grady by fitting the results of an elastic shock and release experiment. It is worth noting that if the data of Manghnani[22] are used to calculate the isothermal elastic loading curve for uniaxial strain and Rayleigh lines are constructed from the initial state to points on the isotherm, a value of 0.74 is obtained for the linear coefficient of Eq. (1). Thus, the use of Eq. (1) appears reasonable. For two specimens (XVI and XVII), no elastic fiducial was measured, apparently due to loss of light in the interferometer. Thus, no HEL or Hugoniot calculations could be performed for them. There was, though, usable data for the reshock and release from the Hugoniot state. Since there were very similar experiments conducted in the release configuration, the Hugoniot states of these two experiments are assumed to be the same as their release counterparts (X and XI) for the strength analysis discussed below.

Since the elastic wave is of large magnitude and the transition between elastic and plastic waves shows considerable variability, the shocked state is analyzed in two steps. First, we integrate the incremental equations for stress and strain

$$\Delta\sigma = \rho_o c \Delta u, \tag{2a}$$

$$\Delta\varepsilon = \Delta u / c, \tag{2b}$$

where $\Delta\sigma$ and $\Delta\varepsilon$ are the increments in stress and strain (both positive in compression), ρ_o is the initial density, and c is the Lagrangian sound speed in the current state. The increment in sample particle velocity, Δu, is calculated[23] from the increment in window velocity using the known response of the LiF window.[24] Equations (2a) and (2b) are used to calculate the loading path until the arrival of the bulk shock, indicated as state No. 1 in Figs. 4 and 5, so that σ_1, ρ_1, ε_1, and u_1 are known.

A Rayleigh line is calculated from state No. 1 to the Hugoniot state based on the Rankine–Hugoniot jump conditions, yielding a slope of

$$\frac{\Delta\sigma}{\Delta u} = \frac{\sigma_h - \sigma_1}{u_h - u_1} = \rho_o U_s^p, \tag{3}$$

where U_s^p is the shock speed of the plastic wave in the Lagrangian reference frame and the subscript h denotes the Hugoniot state. With the known Hugoniot of the impactor (if copper or tantalum) or the known particle velocity for symmetric impact ($u_h = 0.5\, V_{\text{impact}}$), the Hugoniot stress can be calculated. The density is calculated using

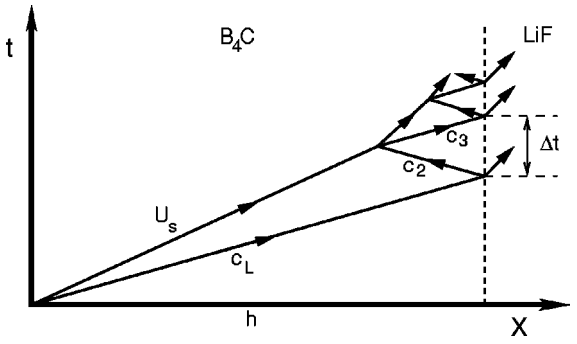

FIG. 6. $X-t$ diagram showing interaction of plastic wave with release wave from sample–window interface.

$$\rho_h = \rho_o \left(\frac{\rho_o}{\rho_1} - \frac{u_h - u_1}{U_s^p} \right)^{-1}. \tag{4}$$

Determining the plastic shock speed is made more difficult by the strong reverberation seen at a particle velocity of about 1 km/s in Fig. 5, which results from the interaction of the elastic precursor, the B_4C/window interface, and the bulk wave. As seen in the $x-t$ diagram in Fig. 6, the plastic wave (U_s in Fig. 6) is perturbed by the release (c_2) from the elastic wave reaching the lower impedance LiF window. The reflection (c_3) of this release wave off the plastic shock is the cause of the reverberations in Fig. 5. These reverberations were significantly more pronounced in powder-gun experiments in Fig. 5 (which have a drop in particle velocity after the HEL) than in the two-stage shots in Figs. 2 and 3 (which have a gradual increase after the HEL), since the drop at the HEL influences the reverberation. Previous researchers[7,17] have attempted to correct for the perturbation. This correction results in a slightly higher shock velocity than is measured for the wave after the reverberation. The shock velocity is calculated from

$$\frac{U_s}{c_L} = \frac{1 - \xi(c_2/c_L)}{1 + \xi}, \tag{5a}$$

where

$$\xi = \frac{c_L c_3 \Delta t}{h(c_2 + c_3)}. \tag{5b}$$

The wave speeds c_L, c_2, and c_3 as illustrated in Fig. 6 are calculated from Eq. (1), h is the initial thickness of the sample, and Δt is the time between the arrival of the elastic wave and the arrival of the first reverberation. In lower-pressure experiments with finite rise times for the first reverberation, Δt is chosen to the midpoint of the rise. The correction of Eq. (5) is typically 2%–3%, though the lowest-pressure tests had larger corrections (6%–8%). It should be noted that after the HEL has been exceeded, B_4C and LiF are relatively well matched in impedance. The shock velocities calculated in this manner are shown in Fig. 7 as a function of particle velocity.

The test parameters and Hugoniot data from the present experiments are given in Table I. Data from these experiments, along with three points of Pavlovskii,[25] those of Gust and Royce[17] (average of two analysis methods), the data of

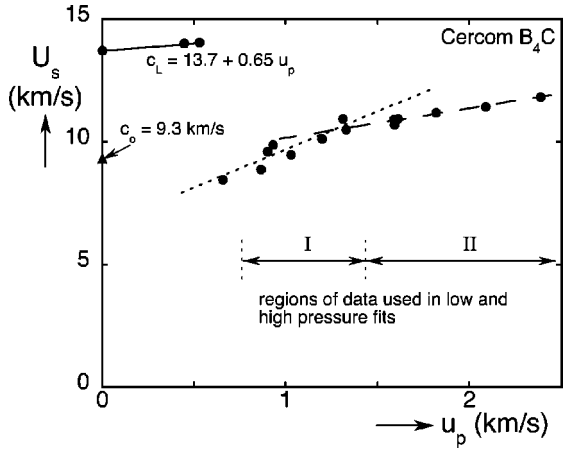

FIG. 7. Shock velocity vs particle velocity for B_4C experiments.

Wilkins,[16] and data from Grady[7] are shown in Fig. 8. The data of Marsh[26] are not included since the material tested had significant porosity. Agreement of data from the different sources is quite good, though the high-pressure data of Grady falls somewhat below that from other sources. Also included in Fig. 8 is a Murnaghan[27] extrapolation relating pressure and specific volume of the form

$$\frac{P}{K_o} = \frac{1}{K_o'}\left(\left(\frac{V_o}{V}\right)^{K_o'} - 1\right), \tag{6}$$

with values of 0.3968 cm^3/g, 234.9 GPa, and 4.26 for initial specific volume (V_o), bulk modulus (K_o), and its first derivative (K_o'), respectively, from ultrasonic measurements[22] to 2.1 GPa. A typical means of determining the strength of material in the shocked state has been to compare a hydrostat to the Hugoniot curve with the difference at a given specific volume proportional to the strength. While this may seem reasonable for B_4C at 20–25 GPa, above 40 GPa this is clearly incorrect as the pressures from Eq. (6) are higher than the Hugoniot stresses. There are two possible explanations for this. First, the extrapolation of the ultrasonic data from 2 GPa to over 50 GPa may result in inaccuracies at high pressures. Second, this is suggestive of a phase transition[5] as discussed in the next section. Since this is essentially the only hydrostat for this material in the literature not based on shock data, the use of reshock and release experiments to estimate strength and the mean stress, as discussed in a later section, is further motivated.

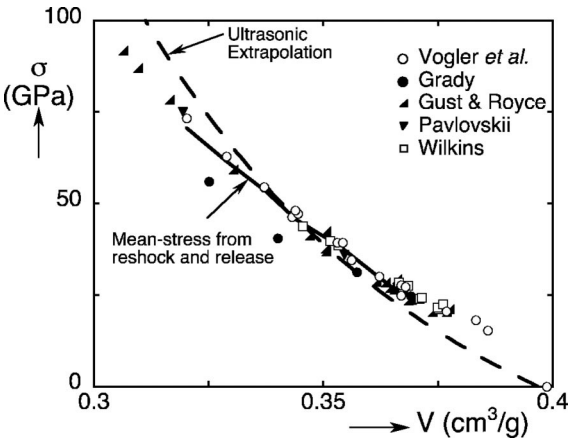

FIG. 8. Stress–volume data from current investigation and other researchers.

Estimates were made for the error in the Hugoniot measurements of Fig. 8. For symmetric impacts, the uncertainty of variables in the Hugoniot state depends primarily upon errors from three sources: the projectile velocity (for calculation of u_p), the particle velocity measured by VISAR (for calculations of state No. 1), and the elastic wave speed. Uncertainties in values of c_o and s of LiF are believed to have an effect too small to be significant. Similarly, inaccuracies due to the use of a Mie–Grüneisen model used for LiF are not included and are believed to be small. The known uncertainty (about 0.2%) of the projectile velocity enters directly into the Hugoniot value for u_h. Uncertainties of approximately 2% in the VISAR measurements result in somewhat different values for σ_1, u_1, and ρ_1. Finally, the uncertainty in the elastic precursor velocity is estimated to be ± 0.3 km/s (about 2%) based on the difference between the ultrasonic and calculated [Eq. (1)] values of c_L as well as observed variations in the ultrasonic value of c_L. Variations in c_L affect the elastic impedance and the shock velocity U_s. The uncertainty of the Hugoniot state (σ_h and ρ_h) was found for each source individually, and the square root of the sum of their squares is taken as the total uncertainty. This corresponds to an assumption of random experimental errors.[28] Relative uncertainties in Hugoniot stress of 1.9%–2.4% are found, with the largest source of error the elastic wave speed c_L. Uncertainties in the specific volume at the Hugoniot state are smaller, 0.2%–0.6%. Error bars for stress in Fig. 8 would be about the size of the symbols, while those for volume would be too small to be distinguished; therefore, neither are shown in Fig. 8.

An additional source of uncertainty is present in nonsymmetric impact, namely the Hugoniot curve for the copper or tantalum impactor. Uncertainties in the Hugoniot data for these materials have been determined,[28] and their effect on the Hugoniot states for experiments BC-I to BC-V was calculated. These uncertainties lead to systematic errors,[28] which are added directly to the square root of the sum of the squares from other sources described above. The result is uncertainties similar to those for symmetric impact: 0.9%–2.2% in the Hugoniot stress, σ_h, and 0.1%–0.4% in the density ρ_h.

IV. PHASE TRANSFORMATIONS

For several years, there has been considerable speculation about the possibility of a phase transition in boron carbide based on shock data[5,7] and Raman spectroscopy.[29] None of these, however, conclusively demonstrated the existence of another phase. Recently, an amorphous phase has been reported for B_4C recovered from ballistic events in which it was loaded to 19–25 GPa,[30] but the size of amorphous zones and, hence, the fraction of materials transformed, was quite small, on the order of 1–3 nm in width. One of the primary goals of this study was to confirm the proposed phase tran-

TABLE II. Linear fits to shock velocity data.

Region	c_o (km/s)	s
I	6.61	3.05
II	8.91	1.22

sitions, if they do exist, or at least place limits on possible volume changes if their existence cannot be confirmed.

An examination of the wave profiles, such as those in Figs. 2, 3, and 5, fails to provide concrete evidence of a first-order phase transition, such as the phase transition wave seen in iron[31] and aluminum nitride[32] or the rarefaction shocks observed upon unloading in calcite.[33] One piece of evidence is that a third wave may be occurring in sample BC-IV at a particle velocity of about 1.4 km/s as seen in Fig. 5. Unfortunately, a precipitous drop in reflected light during the plastic wave makes that data suspect. Another possible piece of evidence is the very steep drop in particle velocity observed during initial unloading of release experiments as seen in Fig. 2. The velocity drop was largest for specimen BC-X. The drop could be due to a transformation back from a higher-pressure phase, which would indicate that the material transforms back immediately upon unloading. However, since the sudden drop is observed immediately upon release for all release experiments from 28–73 GPa, it is more likely to be due to strength effects in the material.

Recently, Grady[7] re-examined the Hugoniot data of Marsh[26] for evidence of phase transitions. Based upon U_s-u_p data for these experiments, three phases were postulated: an ambient phase, a second phase from about 30–50 GPa, and a third phase above 50 GPa. Shock velocity data for the present experiments are shown in Fig. 7. The bilinear nature of the shock data above the HEL in Fig. 7 is obvious, so the data were divided to give the best fit. The elastic data were assumed to follow Eq. (1), while the fit parameters for two linear regions above the HEL are given in Table II. The experiment with the lowest pressure (BC-I) is omitted from this fit as discussed later. The break in the data occurs at a particle velocity of around 1.5 km/s, but the intersection of the linear fits occurs at about 1.25 km/s. The values of stress and particle velocity for the discontinuity are similar but slightly lower than obtained by Grady. Of course, another possible explanation for a discontinuity in slope is a change in the strength behavior of the ceramic. The break can also be seen in the $\sigma-V$ plane in Fig. 8 at about 40 GPa and is seen to have, at most, a volume change of about 3% associated with it (assuming full transformation occurs at a single pressure). Such a small change would be difficult to detect using traditional plate impact techniques. Finally, we note that the ambient bulk sound speed of 9.3 km/s is significantly higher than the intercept value of 6.58 km/s obtained for the linear fit of the low-pressure data. This behavior may be due to a phase transformation or shear softening just above the HEL, though it seems unlikely that strength phenomena are responsible for both the low shock speed just above the HEL and the discontinuity in the shock velocity at 40 GPa. The only other ceramic for which shock velocities lower than the ambient bulk sound speed has been reported is Si_3N_4,[3] a material which is believed to have a phase transition somewhat above the HEL.

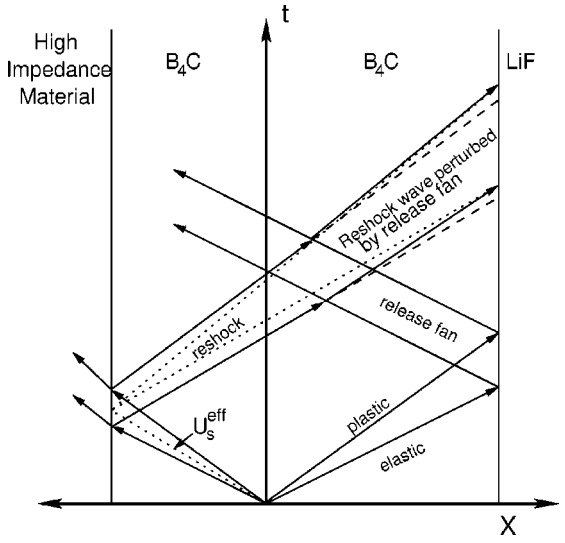

FIG. 9. $X-t$ diagram illustrating wave interaction in reshock and release experiments.

As with previous work, these results are not conclusive regarding the existence of one or more phase transitions. These results are, however, highly suggestive of their existence, and all the experimental data are consistent with their existence. The current data provide a bound on the volume change associated with a possible 40 GPa phase transitions.

V. STRENGTH

The reshock and release experiments were used as part of an effort to identify potential phase transitions in B_4C. As discussed previously, no conclusive evidence of phase transformations was obtained from them. They were also used to assess the shear stress and the residual strength in the shocked state as was done for aluminum,[34] beryllium,[35] and, more recently, alumina.[21] Beginning from the shocked state given in Table I, the stress–strain paths during loading or unloading were estimated using the incremental forms of the conservation equations in Eq. (2). The analysis is approximate in that the unloading/reloading wave emanating from the back of the impactor is assumed to be a single shock (rather than separate elastic and plastic waves) with effective velocity, U_{eff}, shown in an $x-t$ diagram in Fig. 9 and given by

$$U_{\text{eff}}=\sigma_h/(\rho_o u_h), \tag{7}$$

where σ_h and u_h are the stress and particle velocities in the shocked (Hugoniot) state, respectively. This assumption is made in order to simplify the analysis of the wave profiles; its effect on the analysis will be discussed later. Lagrangian sound speeds for use in Eq. (2) are calculated with respect to arrival of this effective wave at the back surface of the impacting B_4C. This analysis method also neglects interactions between the window and sample as the reshock or release reaches it as illustrated in Fig. 9. In the current case, however, the impedances of B_4C and LiF are quite similar in

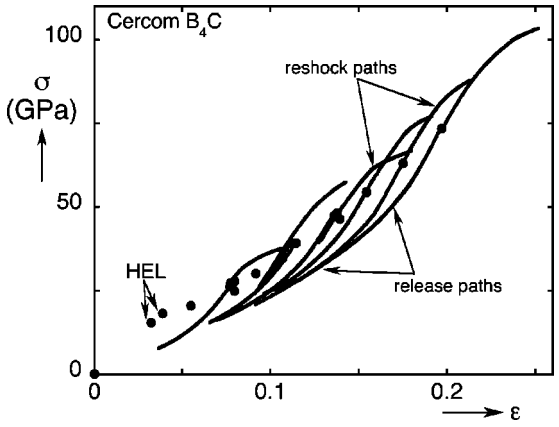

FIG. 10. Loading and unloading paths for reshock and release of B_4C experiments.

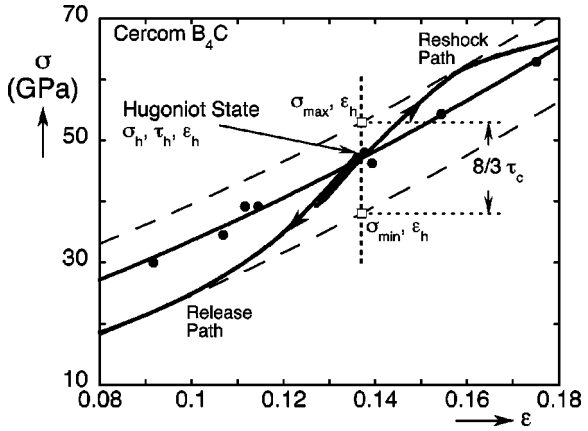

FIG. 11. Illustration of technique used to determine shear stress state and shear strength in the shocked state from reloading and unloading paths.

the shocked state above the HEL. Despite these approximations, the method provides reasonable estimates of the stress–strain paths followed without resorting to a particular constitutive model.

In analyzing release experiments using Eq. (2), reshock experiments proved a bit more difficult to deal with than release experiments. As seen in Fig. 3 and discussed briefly earlier, a small drop in particle velocity precedes the reshock wave. This is due to the low impedance glue bond between the B_4C impactor and the high impedance backing material. A larger release was observed for one experiment, BC-XIII, probably due to the separation of the impactor and backing during projectile launch. Measurements indicate a glue layer thickness of about 7 μm; such a layer will release the impactor to a much lower stress, but will then rapidly ring up. Most of the release fan is quickly overtaken by the reshock wave, but a small part propagates all the way to the window. Similar behavior has been seen in other ceramics,[21,36] and simulations using the hydrocodes CTH[37] and Wondy[38] in which an explicit glue layer is included give releases similar to those observed experimentally. In future experiments, we hope to ameliorate this effect by the use of higher impedance bonds. To account for the unloading, Eq. (2) was integrated for the small release. A small delay time was introduced in the analysis for the entry of the reshock wave into the projectile B_4C. The delay introduced was 7–16 ns for these experiments, which does not seem an unreasonable time for such a glue layer to ''ring up.'' The value of the delay time was adjusted until the slope of the reshock σ–ε curve at σ_h matches that during release; i.e., the sample is assumed to unload and reload elastically so the sound speed at σ_h is a constant. Possible errors associated with the analysis of the release before reloading will be discussed below.

The loading and unloading paths for twelve experiments from their Hugoniot states are shown in Fig. 10. The reshocked samples reach points above the Hugoniot, while the released samples reach stresses below it. In the Hugoniot state, the stress σ_h, mean stress $\overline{\sigma}_h$, and shear stress (τ_h) are related by

$$\sigma_h = \overline{\sigma}_h + 4/3\tau_h . \tag{8}$$

Of course, neither $\overline{\sigma}_h$ nor τ_h can be found using the Rankine–Hugoniot jump conditions. To calculate them using the reshock and release loading paths, upper and lower yield surfaces defined by the two paths are found. The upper and lower yield surfaces are assumed to have the same shape as a quadratic fit to the Hugoniot data above the HEL given by

$$\sigma_h = 7.64 + 182.26\varepsilon + 769.95\varepsilon^2, \tag{9}$$

with units of GPa. The quadratic fit and yield surfaces determined for specimens BC-VIII and BC-XIV are shown in Fig. 11. The stresses where a vertical line from the Hugoniot state will intercept the yield surfaces, denoted by $\sigma_{\max}$ and $\sigma_{\min}$, are defined as

$$\sigma_{\max} = \overline{\sigma}_h + 4/3\tau_c , \tag{10a}$$

$$\sigma_{\min} = \overline{\sigma}_h - 4/3\tau_c \tag{10b}$$

where τ_c is the shear strength of the material in the shocked state. Thus, the shear strength and mean stress are calculated as

$$\tau_c = 3/8(\sigma_{\max} - \sigma_{\min}), \tag{11a}$$

$$\overline{\sigma}_h = (\sigma_{\max} + \sigma_{\min})/2. \tag{11b}$$

Once the mean stress is known, the shear stress in the Hugoniot state, τ_h, can be calculated from Eq. (8). Finally, the shear strength at the Hugoniot state is related to the strength in uniaxial stress Y_h (assuming a von Mises yield function) by

$$Y_h = 2\tau_c . \tag{12}$$

Results calculated with Eqs. (8), (10), (11), and (12) for six sets of experiments are given in Table III, while τ_h and Y_h are plotted versus Hugoniot stress in Fig. 12 along with calculations in the elastic range with a value of 0.16 assumed for ν. The shear stress falls off rapidly above the HEL, retaining only a fraction of that in the elastic regime. This suggests that the material has not failed completely, though τ_h is tending toward zero as the shock stress increases. There also is a modest drop in the strength at the HEL but, thereafter, Y_h increases with shock pressure and eventually reaches a value close to that at the HEL. The data in Table III are similar to that found for alumina using the same

TABLE III. Strength parameters in the Hugoniot state.

Specimens (release/reshock)	σ_h (GPa)	ε_h	$\sigma_{\max}$ (GPa)	$\sigma_{\min}$ (GPa)	$\overline{\sigma_h}$ (GPa)	τ_h (GPa)	Y_h (GPa)
VI/XII	27.5	0.078	30.0	18.7	24.4	2.3	8.5
VII/XIII	39.2	0.113	46.2	30.3	38.2	0.7	11.9
VIII/XIV	47.7	0.137	53.0	38.1	45.5	1.6	11.2
IX/XV	54.4	0.154	62.4	44.4	53.4	0.8	13.5
X/XVI	62.9	0.175	71.3	51.6	61.5	1.1	14.8
XI/XVII	73.3	0.1968	79.9	61.3	70.6	2.0	14.0

techniques,[21] though, in that case, the shear stress was found to drop very close to zero and there appeared to be no drop in Y_h.

The dynamic mean–stress data from these six pairs of experiments is shown in Fig. 8 for comparison with Hugoniot data and the extrapolated hydrostat discussed earlier. The lowest two values are seen to lie slightly above the extrapolated hydrostat, while the upper three values lie increasingly far below it. This is consistent with the presence of a phase transformation at about 40 GPa as discussed above, but additional data are needed to more accurately resolve this stress regime. This technique makes it possible to determine the mean–stress curve for high strength materials and those that go through phase transformations. High strength materials are difficult to test hydrostatically using diamond anvil cell techniques, while phase transformations make extrapolations inaccurate. Since no diamond anvil cell data on B_4C has yet been published and extrapolating low-pressure data is clearly incorrect, the present mean stress data is the most reliable estimate for the hydrostat for pressures above about 35 GPa.

The errors associated with the calculations of the reshock and release paths are difficult to assess. Readily identifiable potential sources of error and uncertainty include: (1) uncertainties in the Hugoniot state and elastic wavespeed, (2) uncertainties in the behavior of LiF, (3) the usage of a single effective shock for the calculation of Lagrangian sound speed [Eq. (7)], (4) the perturbation of the reshock or release wave due to release from the window (see Fig. 9), and (5) complications in analyzing the reshock data due to the release of the glue bond. Each of these potential sources of uncertainty will be discussed in turn. First, the uncertainty in σ_h translates to an uncertainty in the mean stress, $\overline{\sigma_h}$, that is of similar magnitude. In contrast, τ_h or Y_h should only be minimally affected since both $\sigma_{\max}$ and $\sigma_{\min}$ will be changed equally, canceling out one another in Eqs. (8) and (11). Variations in the elastic wave speed affect $\overline{\sigma_h}$ via the uncertainty in the Hugoniot state but do not affect τ_h. Their effect on Y_h should be about 2%. Second, the equation of state of LiF is known quite well, so errors are expected to be of an order typical for Hugoniot data, 1%–2%.

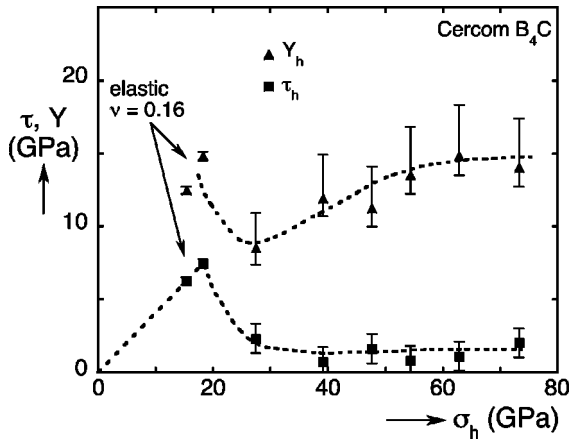

FIG. 12. Shear stress τ_h and strength Y of B_4C in the shocked state estimated from reshock and release experiments.

To assess the effects of the third and fourth points, one-dimensional hydrocode simulations were conducted with CTH[39] and Wondy[38] and the resulting data analyzed with the incremental method. The geometries and velocities were similar to those of the experiments, and two constitutive models were used for B_4C: an elastic-perfectly plastic model and the JH-2 model.[40] These two models provide quite different results, thus allowing the incremental analysis technique to be examined under different conditions. Because both of these models will follow the Hugoniot during reshock, they were not useful for assessing the incremental analysis technique in that condition. Assuming a single shock results in an overestimation of Y_h of 2–4 GPa for both models. Since the effect should be approximately symmetric for reshock and release, it is not expected to affect τ_h significantly. For point four, the release from the window is known to lower the apparent sound speed, making each $\Delta\sigma$ smaller and each $\Delta\varepsilon$ larger [Eq. (2)]. In the σ–ε plane (Fig. 10), this makes release and reshock paths less steep and closer to the Hugoniot. Thus, the values of Y_h in Fig. 10 are conservative and the actual values should be larger. Additional computer simulations suggest that the values calculated herein are 10%–20% lower than the actual values. The analysis of these simulations includes the assumption of a single effective shock (point 3), so this error estimate includes partially canceling errors due to a single effective shock and wave interactions from the window. No attempt has been made to correct for the systematic error due to the window. Since the error should be roughly symmetric for unloading and reloading, the effect upon τ_h and $\overline{\sigma_h}$ should be minimal.

Finally, uncertainties due to the release at the glue bond between the B_4C impactor and the higher impedance backing material can be estimated by analyzing the experimental data differently. For example, if the entire release and reshock is assumed to be caused by the same effective shock (no time delay), the reloading part will be less stiff. This will lower $\sigma_{\max}$, thus increasing τ_h and decreasing $\overline{\sigma_h}$ and Y_h. Even

under these assumptions, the reshock arrives at a speed faster than the bulk sound speed, and the reloading path lies above the Hugoniot. Differences of the order of 1 GPa are found for these quantities when the data are analyzed in this manner. It should be noted that this estimate assumes that most of the release fan from the glue bond is overtaken very rapidly so that most of the B_4C experiences only a modest elastic release. This assumption is confirmed by the hydrocode simulations.

Based upon the discussion above, error bars are shown in Fig. 12 that account for the experimental uncertainties (e.g., c_L) and systematic errors (e.g., wave interactions). Even with the uncertainties shown in Fig. 12, the general conclusions reached for the strength behavior of B_4C are largely unchanged, though it is possible that the material supports no significant shear stress in the Hugoniot state.

This data on the strength of B_4C paint a picture of the behavior of the material different from that previously held. Other researchers[5,6] have indicated that the material loses most or all of its strength in the shocked state. Indeed, τ_h is much lower than would be expected based on the HEL measured. However, the material is able to load or unload elastically from the shocked state, and it is capable of supporting a shear stress comparable to the value at the HEL. It is not clear if the drop in τ_h is due to a phase transformation or if the material is heavily damaged (fractured) in the shocked state but still capable of supporting high shear stresses because of its high intrinsic strength and the high confining pressure. Another outstanding issue is the steadiness of the reshock wave and the possible role of rate and dwell-time effects on the reshock behavior. Future studies will address the evolution of reshock waves through specimens of varying thicknesses.

VI. HETEROGENEOUS DEFORMATION

The possibility of significant heterogeneity in the deformation of B_4C under shock loading has been suggested. Irregularities in single point VISAR readings led to the suggestion[5] that there was heterogeneous deformation with an associated length scale of 50–500 μm. More recent work[8] using the inclined mirror method indicated heterogeneities described as being 10's of micrometers in size. Experiments of the current work display features suggestive of heterogeneous deformation. In Fig. 5, specimens BC-II and BC-III show significant oscillations in the Hugoniot state. The oscillations seen in these specimens have periods of 0.2–0.5 μs. Assuming wave speeds of 14 km/s, this implies feature sizes of 3–7 mm, a rather large size considering the grain size of 15 μm for this material.[2] The oscillations seen in experiments at lower stresses are largely absent at higher stresses. In fact, no significant oscillations are seen for BC-V or any of the specimens tested in the two-stage gun (BC-VI to BC-XV), though this may be partially due to the thinner samples used on the two-stage gun.

In order to directly address the issue of heterogeneous deformation, one experiment (BC-I) was performed with the line–VISAR system, which allows particle velocities to be spatially resolved along a line. For this experiment, measurements were taken every 17 μm along a length of about 640 μm, while the width of the sampled region was approximately 50–100 μm. The specimen was impacted with a tantalum impactor at a velocity of 0.984 km/s, and the average of the line–VISAR measurements ($\overline{u_p}$) is shown in Fig. 5. The average VISAR history from this experiment is quite similar to those of BC-II and BC-III. However, only a single wave is seen after the elastic wave due to the long rise time and the small jump in particle velocity. The value for shock velocity in Table I, 8.45 km/s, was obtained using the pulse-echo analysis described above, which assumes that the wave observed is a reverberation of the elastic wave. If, on the other hand, the second wave is a bulk wave, the shock velocity would be 9.39 km/s (quite close to the ultrasonic bulk sound speed). Due to this ambiguity, the shock velocity of this experiment was not included in the linear U_s-u_p fit in Fig. 7. This uncertainty, however, makes little difference (about 1%) in the stress at the Hugoniot state due to the very high HEL.

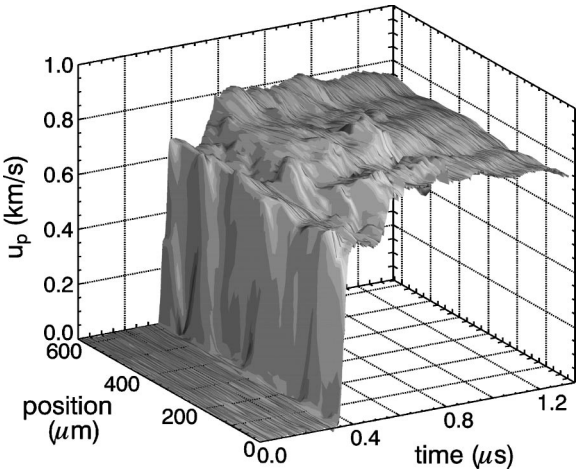

FIG. 13. Spatially resolved particle velocity readings for sample BC-I.

The particle velocity readings for this sample as a function of spatial position are shown in Fig. 13. The elastic wave has a surprisingly uniform particle velocity, but there are significant differences in the arrival times for different parts of the wave. To illustrate this better, the average reading from Fig. 5 is subtracted from the discrete measurements in Fig. 13, with the difference shown in Fig. 14. The arrival time of the wave is seen to vary by as much as $\pm$15 ns, and the characteristic length associated with the variation is approximately 50–100 μm. These variations are believed to be the result of the local elastic anisotropy of B_4C.

Significant variations in particle velocity become apparent after the second wave, and they appear to have both characteristic time and length scales. Several significant deviations from the average can be seen in Fig. 14 at about 0.5 μs, which corresponds to the arrival of the elastic wave. The magnitude of these deviations is somewhat misleading because small differences in the arrival time of the wave result in large deviations since the particle velocity changes very rapidly across the shock front. Additional deviations as large as 100 m/s are seen in the second wave and after the second wave has passed. They are about 100–200 μm in size and on the order of 100 ns in duration. This duration is consistent

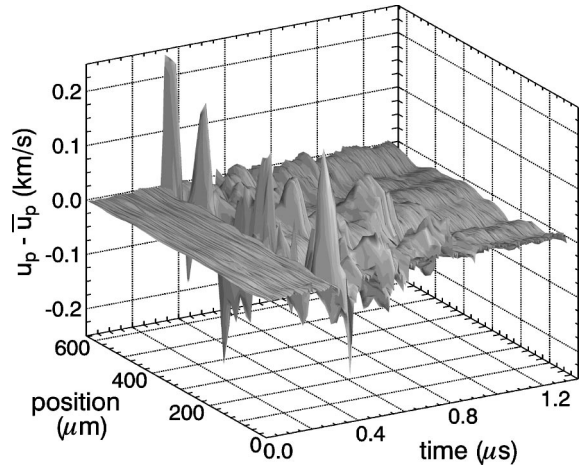

FIG. 14. Deviation of line-VISAR reading from average particle velocity for sample BC-I.

with that seen with conventional VISAR systems as discussed above. These characteristic lengths and times, though, are inconsistent with one another as dividing the former by the latter yields a characteristic velocity on the order of 1–2 km/s, much lower than any waves observed in this material.

These are measurements using the line-VISAR illustrate the heterogeneity of both the elastic and plastic waves in polycrystalline B_4C. In contrast, experiments on single-crystal alumina (sapphire)[41] showed a homogeneous elastic wave and a heterogeneities plastic wave. VISAR measurements are, of course, an integration of the material behavior through the thickness of the specimen, so the measurements will be influenced by all of the grains through the thickness. The elastic wave is relatively uniform despite the highly anisotropic nature of boron carbide grains.[42] It may be that the elastic wave is being ''filtered'' by relatively weaker grains so that the elastic wave measured represents the strength of the weakest grains. Variations in the second wave suggest that a heterogeneous failure process is occurring such as that seen in quartz[43] or that complex local deformation histories are occurring as observed in discrete-element simulations.[44] Of course, nonuniform failure processes would almost certainly give rise to local variations in deformation. If the variations are, in fact, due to a failure process, it may be possible to determine the kinetics of the process by the variation of time and length scales in the heterogeneity with increasing stress.

VII. CONCLUSIONS

A series of planar impact experiments with time-resolved interferometry has been conducted on the ceramic boron carbide. By the use of high or low impedance backing material on the impactor, the reshock and release behavior of the material was also assessed. The Hugoniot data obtained from these experiments agrees reasonably well with the data in the literature. As with previous studies, there are suggestions of one or more phase transitions, but neither the Hugoniot data nor the reshock/release data provide clear evidence of transitions. The experimental data is consistent, though, with a small-volume-change phase transition at a shock stress of about 40 GPa.

Additional data on strength were obtained from the reshock and release experiments. The material was found to display elastic/plastic behavior during both loading and unloading from the shocked state. The paths followed from the Hugoniot state were found using an incremental analysis of the measured velocity histories. From these paths, the shear stress, mean stress, and strength in the shocked state were determined. The shear stress in the shocked state is low, so that the Hugoniot curve nearly corresponds to the dynamic mean stress curve. However, in sharp contrast to other studies on this material, the strength in the shocked state is found to be quite high—of a similar magnitude to the strength at the HEL. The physical explanation for the strength phenomena is unclear but may be due to damage mechanisms during loading and high hydrostatic stress in the shocked state. The mean–stress curve determined from the present experiments differs significantly from the extrapolation of low-pressure data above 50 GPa. Considering the difficulties associated with diamond anvil cell testing of high strength materials, companion reshock and release experiments may be the most appropriate technique to determine the mean–stress behavior of high strength ceramics such as B_4C.

Finally, spatially resolved interferometry measurements were made. Variations in the arrival of the elastic precursor and bulk wave were detected. Also, significant spatial and temporal variations were observed after the passage of the bulk wave. The space and time scales associated with these variations, though, have no clear connections to known microstructural features of the material and are thus of unknown origin.

This investigation has provided one of the most complete data sets on the shock behavior of boron carbide. Unexplained physical phenomena appear to be occurring to create the observed strength behavior of the material. Therefore, additional work is needed to identify the processes controlling the loss and retention of strength in boron carbide. A key part of this behavior may be heterogeneous deformation and, perhaps, damage as observed during the spatially resolved shock experiment on this material.

ACKNOWLEDGMENTS

Sandia is a multiprogram laboratory operated by Sandia Corporation, a Lockheed–Martin Company, for the United States Department of Energy under Contract No. DE-AC04-94AL85000. Helpful conversations with Dennis Grady and Datta Dandekar are gratefully acknowledged.

[1] F. Thévenot, J. Eur. Ceram. Soc. **6**, 205 (1990).
[2] D. P. Dandekar, U.S. Army Research Laboratory, Alberdeen Proving Ground, MD, Report No. ARL-TR-2456 (2001).
[3] D. E. Grady, Mech. Mater. **29**, 181 (1998).
[4] L. C. Chhabildas, W. D. Reinhart, and D. P. Dandekar, in *Ceramic Armor Materials by Design*, edited by J. W. McCauley *et al.* (The American Ceramics Society, Westerville, OH, 2002), pp. 269–278.
[5] D. E. Grady, J. Phys. IV **4**, C8 (1994).
[6] N. K. Bourne, Proc. R. Soc. London, Ser. A **458**, 1999 (2002).
[7] D. E. Grady, Applied Research Associates report to U.S. Army TACOM-

TARDEC, Warren, MI, for Contract No. DAAE07-01-P-L843 for project No. 0778 (2002).
[8] T. Mashimo and M. Uchino, J. Appl. Phys. **81**, 7064 (1997).
[9] W. M. Trott, M. D. Knudson, L. C. Chhabildas, and J. R. Asay, in *Shock Compression of Condensed Matter*, edited by M. D. Furnish *et al.* (American Institute of Physics, Melville, NY, 2000), pp. 993–998.
[10] N. S. Brar, Z. Rosenberg, and S. J. Bless, in *Shock Compression of Condensed Matter*, edited by S. C. Schmidt *et al.* (North–Holland, New York, 1992), pp. 475–478.
[11] J. H. Gieske, T. L. Aselage, and D. Emin, in *Boron-Rich Solids*, edited by D. Emin *et al.* (American Institute of Physics, New York, 1991), pp. 376–379.
[12] W.-D. Winkler and A. J. Stilp, in *Shock Compression of Condensed Matter*, edited by S. C. Schmidt *et al.* (North–Holland, New York, 1992), pp. 475–478.
[13] J. R. Asay, L. C. Chhabildas, and L. M. Barker, Sandia National Laboratories, Albuquerque, NM, Report No. SAND85-2009 (1985).
[14] J. L. Wise and L. C. Chhabildas, in *Shock Waves in Condensed Matter*, edited by Y. M. Gupta (Plenum, New York, 1986), pp. 441–454.
[15] L. M. Barker and R. E. Hollenbach, J. Appl. Phys. **43**, 4669 (1972).
[16] M. L. Wilkins, Lawrence Radiation Laboratory, Livermore, CA, Report No. UCRL-50460 (1968).
[17] W. H. Gust and E. B. Royce, J. Appl. Phys. **42**, 276 (1971).
[18] J. R. Asay, G. R. Fowles, G. E. Duvall, M. H. Miles, and R. F. Tinder, J. Appl. Phys. **43**, 2132 (1972).
[19] T. Mashimo, in *Shock Waves in Materials Science*, edited by A. B. Sawaoka (Springer, New York, 1993), pp. 113–144.
[20] W. D. Reinhart, L. C. Chhabildas, D. E. Grady, and T. Mashimo, in *Ceramic Armor Materials by Design*, edited by J. W. McCauley *et al.* (The American Ceramics Society, Westerville, OH, 2002), pp. 233–247.
[21] W. D. Reinhart and L. C. Chhabildas, Int. J. Impact Eng. **29**, 601 (2003).
[22] M. H. Manghnani, Y. Wang, F. Li, P. Zinin, and W. Rafaniello, in *Science and Technology of High Pressure*, edited by M. H. Manghnani *et al.* (Universities Press, Hyderabad, India, 2000), pp. 945–948.
[23] J. Lipkin and J. R. Asay, J. Appl. Phys. **48**, 182 (1977).
[24] W. J. Carter, High Temp. - High Press. **5**, 313 (1973).
[25] M. N. Pavlovskii, Sov. Phys. Solid State **12**, 1737 (1971).
[26] S. P. Marsh, *LASL Shock Hugoniot Data*. (University of California Press, Berkley, CA, 1980).
[27] F. D. Murnaghan, *Finite Deformation of an Elastic Solid* (Wiley, New York, 1951).
[28] A. C. Mitchell and W. J. Nellis, J. Appl. Phys. **52**, 3363 (1981).
[29] V. Domnich, Y. Gogotsi, M. Trenary, and T. Tanaka, Appl. Phys. Lett. **81**, 3783 (2002).
[30] M. Chen, J. W. McCauley, and K. J. Hempker, Science **299**, 1563 (2003).
[31] D. Bancroft, E. L. Peterson, and S. Minshall, J. Appl. Phys. **27**, 291 (1956).
[32] M. E. Kipp and D. E. Grady, J. Phys. IV **4**, C8 (1994).
[33] D. E. Grady, in *Shock Waves in Condensed Matter*, edited by Y. M. Gupta (Plenum, New York, 1986), pp. 589–593.
[34] J. R. Asay and L. C. Chhabildas, in *Shock Waves and High-Strain-Rate Phenomena in Metals*, edited by M. A. Meyers and L. E. Murr (Plenum, New York, 1981), pp. 417–431.
[35] L. C. Chhabildas, J. L. Wise, and J. R. Asay, AIP Conf. Proc. **78**, 422 (1982).
[36] D. P. Dandekar, W. D. Reinhart, and L. C. Chhabildas, J. Phys. IV **110**, 827 (2003).
[37] F. J. Zeigler, J. M. McGlaun, S. L. Thompson, and T. G. Trucano, Sandia National Laboratories, Albuquerque, NM, Report No. SAND87-0725C (1987).
[38] M. E. Kipp and R. J. Lawrence, Sandia National Laboratories, Albuquerque, NM, Report No. SAND81-0930 (1982).
[39] J. M. McGlaun, S. L. Thompson, and M. G. Elrick, Int. J. Impact Eng. **10**, 351 (1990).
[40] G. R. Johnson and T. J. Holmquist, J. Appl. Phys. **85**, 8060 (1999).
[41] W. D. Reinhart, L. C. Chhabildas, W. M. Trott, and D. P. Dandekar, in *Shock Compression of Condensed Matter*, edited by Y. Horie (American Institute of Physics, Melville, New York, 2001), pp. 775–778.
[42] K. J. McClellan, F. Chu, and J. M. Roper, J. Mater. Sci. **36**, 3403 (2001).
[43] P. J. Brannon, C. H. Konrad, R. W. Morris, E. D. Jones, and J. R. Asay, J. Appl. Phys. **54**, 6474 (1983).
[44] K. Yano and Y. Horie, Phys. Rev. B **59**, 13672 (1999).